The Astrophysical Journal, 913:43 (14pp), 2021 May 20 https://doi.org/10.3847/1538-4357/abf55e

Evidence for an MHD Disk Wind via Optical Forbidden Line Spectroastrometry*

E. T. Whelan[1], I. Pascucci[2], U. Gorti[3], S. Edwards[4], R. D. Alexander[5], M. F. Sterzik[6], and C. Melo[7]
[1] Maynooth University Department of Experimental Physics, National University of Ireland Maynooth, Maynooth, Co. Kildare, Ireland
[2] Lunar and Planetary Laboratory, The University of Arizona, Tucson, AZ 85721, USA
[3] SETI Institute/NASA Ames Research Center, Mail Stop 245-3, Moffett Field, CA 94035-1000, USA
[4] Five College Astronomy Department, Smith College, Northampton, MA 01063, USA
[5] School of Physics & Astronomy, University of Leicester, Leicester, LE1 7RH, UK
[6] European Southern Observatory, Karl-Schwarzschild-Str. 2, D-85748, Garching, Germany
[7] European Southern Observatory, Alonso de Córdova 3107, Vitacura, Casilla 19001, Santiago de Chile, Chile
Received 2021 February 14; revised 2021 April 5; accepted 2021 April 5; published 2021 May 24

Abstract

Spectroastrometry is used to investigate the low-velocity component (LVC) of the optical forbidden emission from the T Tauri stars RU Lupi and AS 205 N. Both stars also have high-velocity forbidden emission, which is tracing a jet. For AS 205 N, analysis reveals a complicated outflow system. For RU Lupi, the [O I] λ6300 and [S II] $\lambda\lambda$6716,6731 LV narrow component (NC) is offset along the same position angle (PA) as the high-velocity component but with a different velocity gradient than the jet, in that displacement from the stellar position along the rotation axis is decreasing with increasing velocity. From the LVC, NC, PA, and velocity gradient, it is inferred that the NC is tracing a wide-angled magnetohydrodynamic (MHD) disk wind. A photoevaporative wind is ruled out. This is supported by a comparison with a previous spectroastrometric study of the CO fundamental line. The decrease in offset with increasing velocity is interpreted as tracing an increase in the height of the wind with increasing disk radius. This is one of the first measurements of the spatial extent of the forbidden emission line LVC NC ($\sim$40 au, 8 au for RU Lupi in the [S II] λ6731 and [O I] λ6300 lines) and the first direct confirmation that the LVC narrow component can trace an MHD disk wind.

Unified Astronomy Thesaurus concepts: Interstellar medium wind (848); Star formation (1569); Stellar jets (1607); Stellar accretion disks (1579)

1. Introduction

A crucial step in understanding how stars accrete their mass, as well as how disks evolve, is clarifying how the accreting disk gas loses angular momentum. Originally magnetohydrodynamic (MHD) disk winds were favored (Koenigl & Ruden 1993) but the prevailing view for several decades has been that magentorotational instability (MRI)-induced turbulence (Balbus & Hawley 1991) leads to outward viscous transport of angular momentum (Armitage 2011), enabling the disk material to flow radially inward. However, recent simulations find that nonideal MHD effects suppress MRI over a large range of disk radii ($\sim$1–30 au), restoring radially-extended MHD disk winds as the prime means for extracting angular momentum and enabling accretion at the observed rates (Bai & Stone 2013; Gressel & Pessah 2015).

On the observational side, there has been renewed interest in identifying disk wind tracers and testing the emerging paradigm of disk evolution. See Ercolano & Pascucci (2017) for a recent review. Emission from optical forbidden lines has been a long-established tracer of flowing material from young stars (Edwards et al. 1987) and recent observations have helped clarify its origin. The so-called "high-velocity" component (HVC), emission blueshifted by $>30\,\mathrm{km\,s^{-1}}$ (Hartigan et al. 1995), is confirmed to be associated with collimated microjets (e.g., Hartigan & Morse 2007) and its [O I] λ6300 luminosity is found to be better correlated with accretion luminosity than with stellar luminosity or mass (Nisini et al. 2018). High-resolution ($\Delta v < 10\,\mathrm{km\,s^{-1}}$) spectroscopy revealed that the low-velocity component (LVC) can be often described as the combination of two Gaussian profiles (a "broad component;" BC; and a "narrow component;" NC; Rigliaco et al. 2013; Simon et al. 2016; McGinnis et al. 2018). The LVC–BC blueshifts and large FWHMs point to an MHD disk wind origin (Simon et al. 2016) while the origin of the LVC–NC is less certain. However, two observables suggest that the NC most likely traces the same MHD wind, instead of a photoevaporative thermal wind (Weber et al. 2020): (i) its peak centroids and FWHMs correlate with those of the BC (Banzatti et al. 2019) and; (ii) the observed [S II] λ6731 LVC luminosities are much weaker than predicted in photoevaporative winds (Pascucci et al. 2020). Clarifying whether the NC truly traces an MHD disk wind and measuring its vertical extent is critical to estimate wind mass-loss rates (Fang et al. 2018) and directly test one of the main predictions of the disk wind theory, i.e., that wind mass-loss rates are similar to mass accretion rates.

Here, we apply the spectroastrometry (SA) technique to the optical forbidden lines from RU Lupi and AS 205 N, two well-known late K-type stars with evidence for jets and winds (see Section 2.1 and Table 1 for further details). Both of our targets are among a handful of TTS with high accretion rates that also show strong [O I] λ6300 with very broad high-velocity emission that is blended with the low-velocity emission, and a low-velocity component that includes both an NC and a broad BC component, where the NC dominates over the BC. Moreover, in contrast to the majority of accreting TTS where the LVC is not detected in [S II] λ6731, our two targets show prominent LVC emission at [S II] λ6731 as well as [O I] λ6300. RU Lupi and AS 205 N have previously been investigated with SA (Takami et al. 2001, 2003) and the results of these works are discussed in Sections 2.1 and 3. While the results presented

* Based on data collected by UVES (089.C-0299(A), 089.C-0299(B), P.I. I. Pascucci) observations at the VLT on Cerro Paranal (Chile) which is operated by the European Southern Observatory (ESO).

Table 1
Spectroastrometric Sample: Properties Relevant to This Study

Object	SpTy	Log($\dot{M}_{acc}$) ($M_\odot$ yr^{-1})	Disk Type	Position Angle (PA)[a] (°)	Disk Inc (°)	Wind Diagnostic	References
RU Lup	K7	−7.77	full	121	19	CO, [O I]	Hu18, C11, P11, F18
AS 205 N	K5	−6.58	full	114	20	CO, [O I]	K18, F18, P11
AS 205 S	K7	⋯	⋯	110	66	⋯	K18

Notes. References stand for: C11 = Curran et al. (2011); F18 = Fang et al. (2018); Hu18 = Huang et al. (2018); P11 = Pontoppidan et al. (2011); K18 = Kurtovic et al. (2018).
[a] This is the position angle of the disk major axis. The most recent values are given here and therefore in some cases they differ from the slit PAs chosen to be parallel to the disk PAs (see Section 2.2 and Table 2).

here confirm the previous results, the much improved spectral resolution and positional uncertainty of our study allowed new details to be revealed about the kinematics and spatial properties of the line regions under investigation. Furthermore, Takami et al. (2003) did not investigate the FELs of the AS 205 system but analyzed several permitted lines (including Hα) to search for a binary signal.

SA is a powerful technique for recovering spatial information from spectra below the angular resolution limitations of the observations (Bailey 1998; Whelan & Garcia 2008; Cahill et al. 2019). Therefore, our goal is to use this technique to explore the origin of the low-velocity forbidden emission in both stars. The technique is based on measuring the centroid of the spatial profile of an emission line region as a function of wavelength and with respect to the centroid of the spatial profile of the continuum. Frequently, this has been done using Gaussian fitting to produce what is referred to as a position spectrum. For ground-based spectroscopy the accuracy to which this can be done is dependent on the signal-to-noise ratio (S/N) of the observation and the seeing, and submilliarcsecond precision has been achieved at near-infrared wavelengths with, for example, VLT/CRIRES (Pontoppidan et al. 2011). This study focuses on the [O I] λ5577, [O I] λ6300, and [S II] λ6731 lines, and the work is organized as follows. In Section 2 the targets, observations, and reduction of the data are described. In Section 3 the spectra and spectroastrometric results are discussed. Sections 4 and 5 are devoted to the Discussion and Summary.

2. Targets, Observations, and Data Reduction

2.1. Targets

RU Lupi is a CTTS located in the Lupus Star-forming region at $d \approx 140$ pc. Takami et al. (2001) used spectroastrometry to investigate the Hα emission of RU Lupi and found that there is a distinct spatial symmetry in the offset for blue and redshifted wings of the Hα line. This signal was attributed to a bipolar outflow driven by RU Lupi and the bipolar outflow theory was supported by their spectroastrometric study of the [O I] λ6300 and [S II] λ6731 lines. The PA of the outflow was estimated at around 225° from this work. Pontoppidan et al. (2011) measure a spectroastrometric signal in the CO fundamental line consistent with that of a wide-angle molecular wind. The DSHARP study measured the PA of the RU Lupi disk at ∼121° (Huang et al. 2018), which is approximately perpendicular to the outflow direction estimated by Takami et al. (2001).

AS 205 is a triple system (AS 205 N, AS 205 Sa,b) (Kurtovic et al. 2018), located in the northern region of the Ophiuchus star-forming region at $d \sim 127$ pc (Gaia Collaboration et al. 2018). Its primary star AS 205 N (also AS 205 A) is a CTTS and it is distinguished by its bright molecular emission (Salyk et al. 2008). AS 205 N and AS 205 S have been detected at a projected separation of 1.″3 and a PA of ∼212° (McCabe et al. 2006). The DSHARP study measures disk PAs of $114° \pm 12°$ and $110° \pm 2°$ for AS 205 N and AS 205 S, respectively (Kurtovic et al. 2018).

Pontoppidan et al. (2011) found evidence for a molecular wind using spectroastrometry in the CO fundamental line. Takami et al. (2003) carried out a spectroastrometric study of the Hα emission from the AS 205 system. Analysis showed a displacement along a PA of ∼33° (E of N), which is interpreted as a binary signature. The authors suggest that any difference between the PA of the displacement and the PA of AS 205 N and AS 205 S can be explained by the orbital motion of the system.

2.2. Observations and Data Reduction

Spectra of RU Lupi and AS 205 were collected with the Ultraviolet and Visual Echelle Spectrograph (UVES) on the European Southern Observatory's (ESO) Very Large Telescope in 2012 May and June (Dekker et al. 2000) through the ESO program 089.C-0299 (PI. I. Pascucci). The wavelength range was approximately 5000–7000 Å and a spectral resolution of $R = 40{,}000$ was achieved. As the spectroastrometric precision is given by the following equation

$$\sigma = \frac{\mathrm{FWHM}}{2.35\sqrt{N_p}} \quad (1)$$

where N_p is the number of detected photons and the FWHM is the seeing. The exposure times were set, assuming typical seeing, to reach 2 mas precision. This goal was achieved and sub 2 mas precision was reached, in general, for the emission line regions. Additional details on the observations are given in Table 2.

The slit width was set to 1″. With UVES it is possible to rotate the slit PA to any position on the sky. For both of our targets, spectra were obtained at four orthogonal slit PAs. The slit PAs were chosen so that spectra were obtained parallel and antiparallel to the known accretion disk PA[8] and parallel and antiparallel to any outflow emission. It was assumed that the PA of any outflow emission is perpendicular to the disk PA. The strategy of obtaining four perpendicular slit PAs is integral to the spectroastrometric analysis. First, the observations at antiparallel slit PAs allow for spectroastrometric artifacts to be ruled out (Brannigan et al. 2006; Whelan et al. 2015). Second, spatial offsets measured in spectra taken at perpendicular slit PAs can be combined to recover the on-sky PA of the

[8] Note that the disks PAs were subsequently updated by the DSHARP study. This is the reason for the difference between the disk PAs given in Table 1 and the slit PAs in Table 2.

Table 2
Observing Log

Object	R.A. (J2000) (J2000)	Decl. (J2000) (J2000)	Date (dd-mm-yyyy)	Slit PA (°)	Exposure Times (ncycle × s)	Seeing (arcsec)
RU Lupi	15:56:42.3	−37:49:15.5	29-06-2012	80	5 × 300	1.3
			28/29-06-2012	170	10 × 300	1.2
			29-06-2012	260	5 × 300	1.0
			28/29-06-2012	350	10 × 300	1.4
AS 205	16:11:31.4	−18:38:28.3	02-05-2012	55	6 × 300	0.77
			02-05-2012	145	6 × 300	0.76
			02-05-2012	235	6 × 300	0.8
			02-05-2012	325	6 × 300	0.68

Table 3
Classification of the [O I] λ5577, [O I] λ6300, and [S II] λ6731 Lines

Object	Line	LVC–NC V_{rad}, FWHM (km s^{-1})	LVC–BC V_{rad}, FWHM (km s^{-1})	HVC Blue V_{rad}, FWHM (km s^{-1})	HVC Red V_{rad}, FWHM (km s^{-1})
RU Lup	[O I] λ6300	−13, 18.2		−66.11, 149.9 (**HVC1**)	
				−197.5, 84.5 (**HVC2**)	
	[S II] λ6731	−23.9, 26.6		−100.1, 157.1 (**HVC1**)	
				−194.71, 59.5 (**HVC2**)	
AS 205 N	[O I] λ6300	−2.35, 16.8		−30.3, 88.2 (**HVC1**)	139.5, 13.7 (**HVC3**)
				−226.5, 76.4 (**HVC2**)	
	[S II] λ6731	−27.3, 16.3		−62.3, 39.8 (**HVC1**)	119.8, 16.1 (**HVC3**)
				−259.2, 35.6 (**HVC2**)	
AS 205 S	[O I] λ6300		−2.6, 42.9		

Note. the bold values indicate the number of high-velocity components (HVCs) in each case.

extension in the emission line region. Further details on the observations are given in Table 2.

The data were initially reduced using the ESO pipeline. Whelan et al. (2015) discuss how the rebinning of X-Shooter spectra by the ESO pipeline can introduce a false spectro-astrometric signal due to a spatial aliasing effect. A similar problem was found for some of the observations when the 2D spectra produced by the UVES pipeline were analyzed using SA. For this reason the spectra were also reduced using standard IRAF routines for the reduction of echelle spectra and it was this data that was used in the analysis and that is presented below. It was found by the authors that using IRAF for the data reduction reduced the spatial aliasing problem. The SA analysis was done using standard fitting routines. The continuum subtraction was done using the IRAF *continuum* routine. With this routine the continuum is fitted and removed from the spectrum row by row, where a row is along the dispersion direction (Whelan & Garcia 2008). For each row only the continuum emission is fitted by masking the emission line regions. The spectra were also also corrected for telluric and photospheric lines using the method outlined in Hartigan et al. (1995) and adopted in subsequent papers (e.g., Rigliaco et al. 2013; Banzatti et al. 2019).

3. Results

The UVES spectra cover two oxygen forbidden lines, one at 6300 Å and the other at 5577 Å, with the latter being the weaker of the two (e.g., Simon et al. 2016), and the sulfur forbidden line doublet at 6716, 6731 Å. The oxygen profiles from both sources, obtained at a resolution similar to UVES, were previously analyzed in Fang et al. (2018) and Banzatti et al. (2019). These works separated CTTS line profiles into distinct kinematic components by finding the minimum number of Gaussian profiles that reproduce the observed one. Components are identified as HVCs, where the absolute value of the Gaussian velocity centroid is larger than 30 km s^{-1}, or LVCs with centroids within 30 km s^{-1} of the photospheric velocity. The LVC can be further decomposed into a BC or NC (FWHM larger or smaller than 40 km s^{-1}), see, e.g., Simon et al. (2016). In those studies both RU Lupi and AS 205 N were found to have quite broad HVC emission, requiring fits with more than one component, and their LVC showed both BC and NC.

We follow a similar approach here. Based on this approach, both [O I] lines of RU Lupi and AS 205 N have an LVC and two (RU Lupi) or three (AS 205 N) HVC components in the [O I] λ6300 transition. For both stars only an LVC NC is identified. A similar decomposition scheme is applied to the [S II] lines (see Table 3).[9] The fits to the [O I] λ6300 and [S II] λ6731 lines are shown in Figures 1 and 3 and the kinematic results presented in Table 3. All velocities quoted here are in the stellocentric reference frame. The differences between the results of the kinematical fitting presented here, and those of previous studies, for the [O I] λ6300 line, are explained by variability in the HVC and this is discussed in detail in the Appendix.

As described in Section 2.1 the AS 205 system is a multiple system with three known members. The aim here was to investigate the emission from AS 205 N. However, for the 55° and 235° slit PAs AS 205 S a,b are also included in the UVES slit. Therefore, given a separation of 1.″3 between the N and S components, and a seeing of ∼0.″8, the emission from AS 205 S could also be evaluated at these PAs (although

[9] Where the [O I] λ6300 and [S II] λ6731 lines are detected the same profiles are seen in the [O I] λ 6363 and [S II]λ 6716 lines, albeit at a lower S/N.

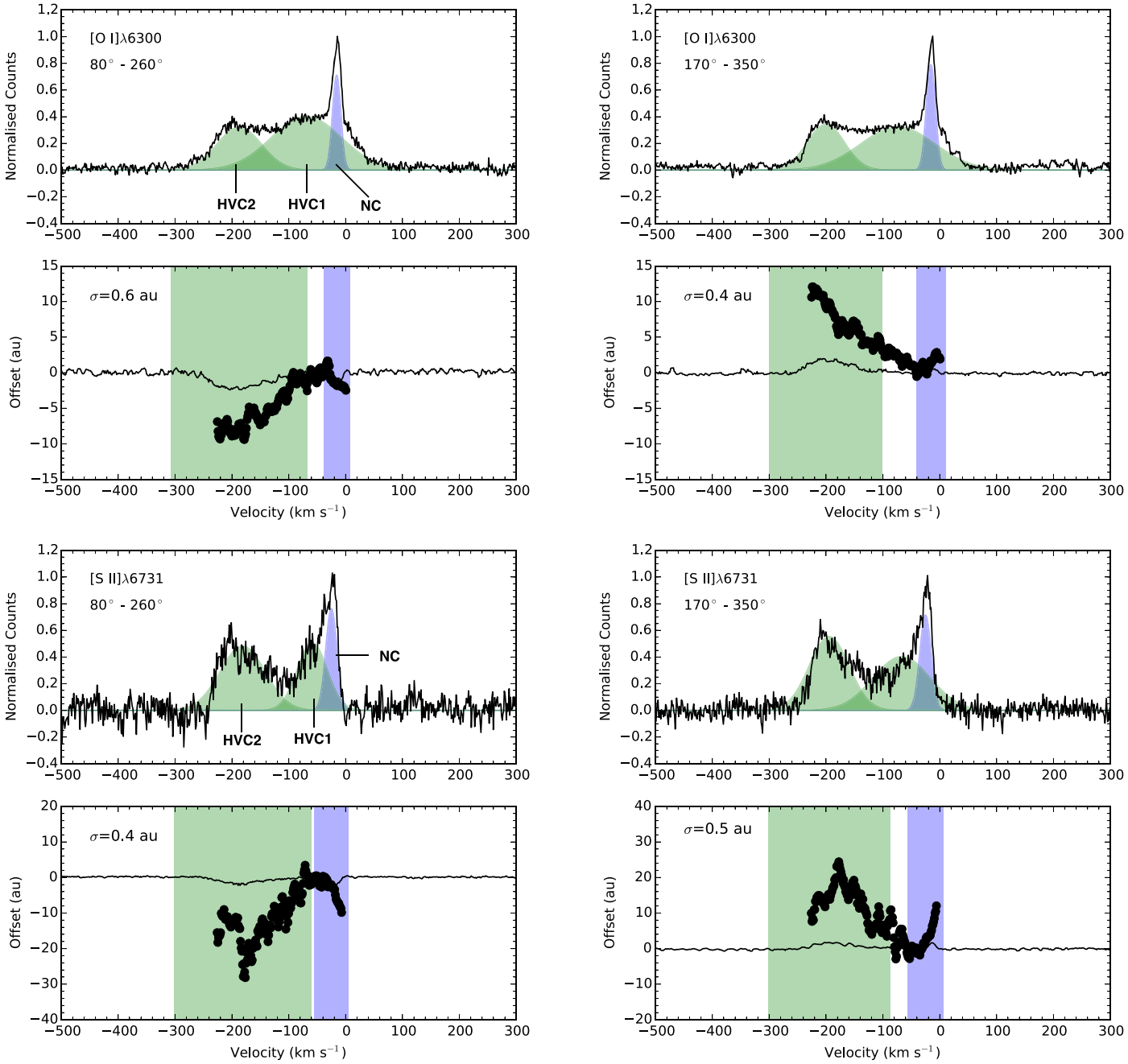

Figure 1. RU Lupi: spectroastrometric analysis of the [O I]λ6300 and [S II]λ6731 lines. Top: the continuum subtracted line emission, normalized to the line peak. The fitted kinematic components are overplotted with with the LVC–NC shown in blue and the HVCs in green. Bottom: the position spectra with the ranges of the LVC–NC and HVC shown as the colored shaded regions. The continuum subtracted offsets are overplotted in black.

AS 205 S a,b are not resolved). For AS 205 S only the [O I] λ6300 line was detected, showing a weak LVC–BC. The spectroastrometric analysis for AS 205 S will be discussed in a separate paper. As the binary PA is $\sim$212° and the slit width was 1″, there was no emission from AS 205 S in the 145° and 325° spectra.

Next, we will be presenting the spectroastrometric results and the following points should be noted for all the results.

1. The method of Takami et al. (2001) where the position spectra for the antiparallel slit positions were subtracted was followed. Takami et al. (2001) discuss how this technique can remove artifacts caused by, for example, optical distortion introduced by the spectrograph, misalignment of the spectrum within the CCD columns, or imperfect flat fielding.
2. The 1σ uncertainties in the centroid position given in Figures 1 and 3 are the average values for the whole spectral range analyzed. The precision will increase at the emission line peaks due to an increase in the S/N.
3. The continuum contamination was removed using the continuum subtraction method outlined in Section 2.2. Position spectra before and after continuum subtraction are shown.
4. The spectroastrometric analysis shown in Figures 2 and 4 does not provide any information on the width (disk

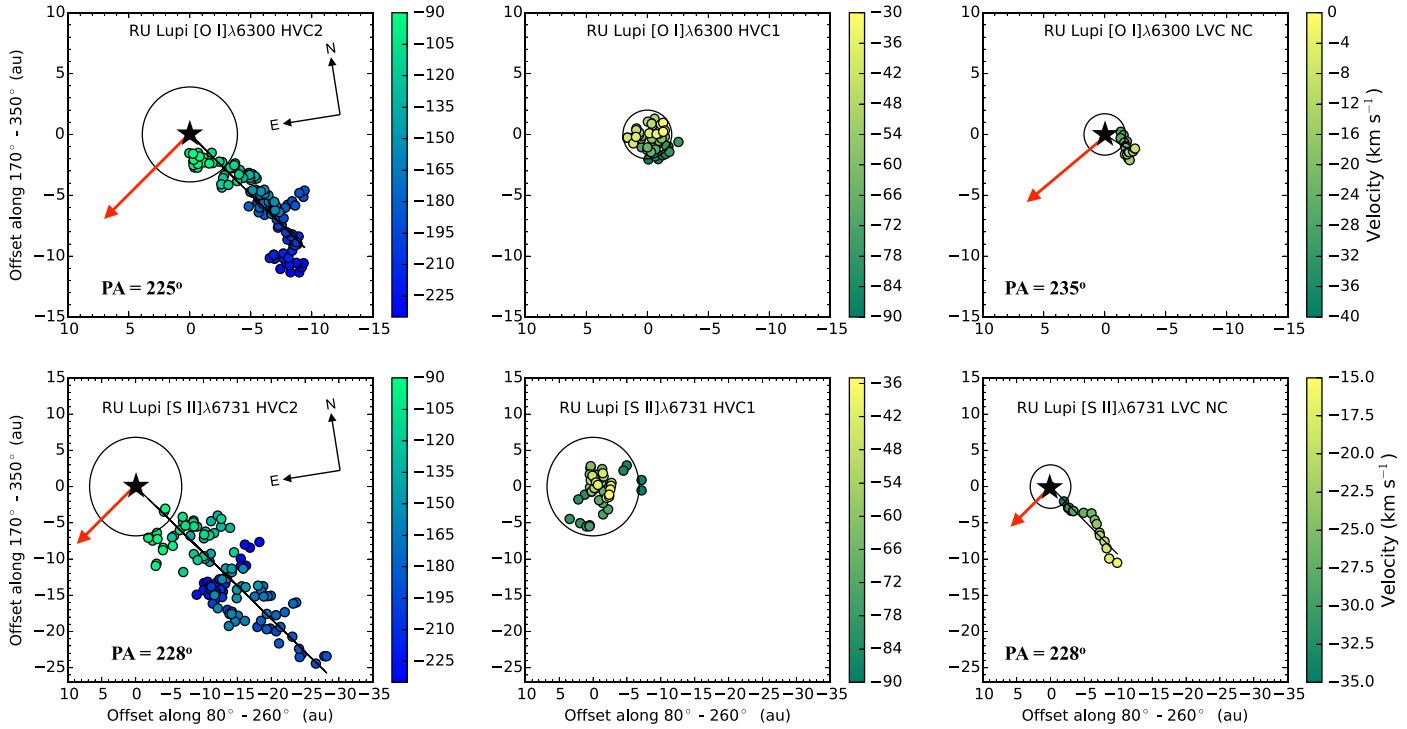

Figure 2. RU Lupi: combining the perpendicular slit PAs to recover the 2D centroid at each wavelength (velocity). The continuum emission has been subtracted here to reveal the full displacement in the outflow. The black circle is the 3σ uncertainty in the centroid, the black line is the best fit PA to the flows, and the red arrow is the PA of the RU Lupi disk major axis.

radial extent) of the flow, as the spectroastrometric centroid measures only the position of the brightest part of the emission region. Any spread perpendicular to the jet PA (black line) is related to the accuracy to which the emission centroid is measured. Spectra taken perpendicular to the jet axis would be required to recover the flow width.

3.1. RU Lupi: A Vertically Extended LVC–NC

For RU Lupi only the blueshifted outflow is detected in forbidden emission and vertical offsets from the star-disk plane are measured in the [O I] λ6300 and [S II]λ6731, λ6716 lines (see Figure 1 where the [O I] λ6300 and [S II] λ6731 results are shown). No spectroastrometric signal is measured in the highest critical density ($\sim 10^8$ cm^{-3}) [O I] λ5577 line. The 1σ uncertainty in the SA can be taken as an upper limit on the extent of the [O I] λ5577 emission region. For RU Lupi this is 3 au (after continuum subtraction), which equals 9 au when the inclination of the system is accounted for. For both the [O I] and [S II] lines it is found that the LVC–NC and the HVC2 are displaced from the stellar position while the HVC1 is coincident with the stellar position (within the uncertainty of the centroid fitting). Note that the [S II] λ6731 emission is more extended than the [O I] λ6300 emission for both the LVC and HVC2, as would be expected due to the lower critical density of the [S II] λ6731 line ($\sim 2 \times 10^4$ cm^{-3}) with respect to the [O I] λ6300 ($\sim 2 \times 10^6$ cm^{-3}). The PA of the extended emission can be recovered by combining the results after continuum subtraction for the perpendicular slit positions. This is shown in Figure 2 with a black line. The LVC–NC, HVC1, and HVC2 are shown separately. It is clear that the HVC1 is not extended and we suggest that it is tracing the outflow close to it launching point. An average PA of $229° \pm 10°$ is measured for the extended emission in agreement with the spectroastrometric analysis of Takami et al. (2001). These results reveal two important properties of the LVC–NC. First, the LVC–NC is extended along the same PA as the HVC2 for both the [O I] λ6300 and [S II] λ6731 lines. This rules out its origin in the disk and connects it to the jet. Second, the velocity gradient for the NC emission is opposite to that of the HVC2: while there is a clear pattern of an increase in offset with velocity in the HVC2, the slower LVC–NC emission is offset further from the star. The meaning of these features are discussed in Section 4.

3.2. AS 205: A Multiple System

As described in Section 2.1 the AS 205 system is a multiple system with three known members. The aim here was to investigate the low-velocity emission from AS 205 N. However, for the 55° and 235° slit PAs AS 205 S a,b are also included in the UVES slit. Therefore, the emission from AS 205 S could also be considered (keeping in mind that As 205 S a,b is not resolved). Considering the disk PA for AS 205 N of 114° and the binary PA of 212°, a complication with interpreting any spectroastrometric signal becomes apparent. As any outflow would be expected to be launched approximately perpendicular to the accretion disk, and as the binary PA is also approximately perpendicular to the AS 205 N accretion disk, it will be difficult to distinguish a binary signal from an outflow signal. However, it would be reasonable to assume that any forbidden emission is originating in an outflow.

For AS 205 N both blue and redshifted displacements are detected in the forbidden emission lines. Again the [O I] λ5577 emission region is not found to be displaced

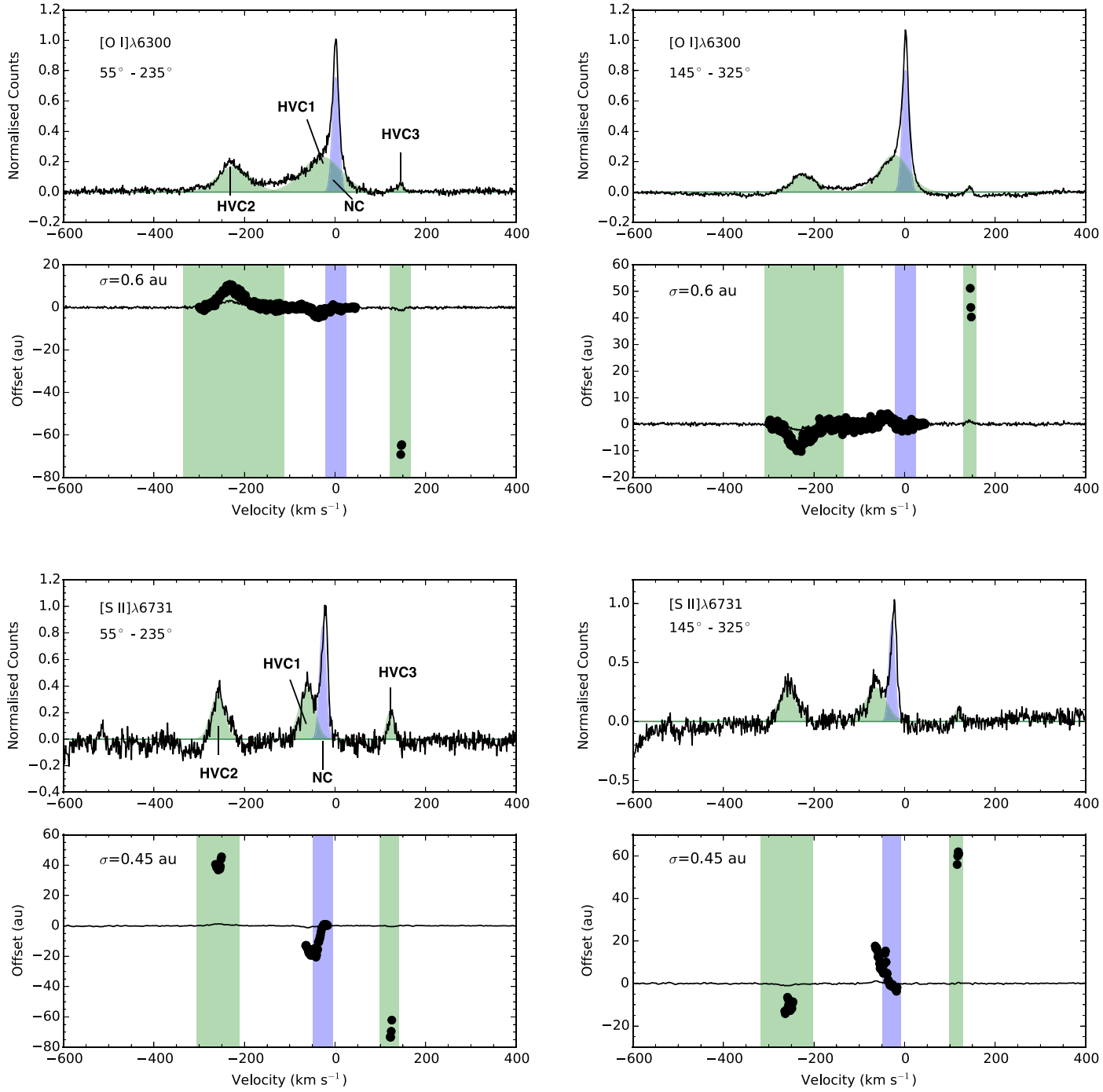

Figure 3. AS 205: spectroastrometric analysis of the [O I]λ6300 and [S II]λ6731 lines. Top: the continuum subtracted line emission, normalized to the line peak. The fitted kinematic components are overplotted with with the LVC–NC shown in blue and the HVCs in green. Bottom: the position spectra with the ranges of the LVC–NC and HVCs shown as the colored shaded regions. The continuum subtracted offsets are overplotted in black.

and the 1σ uncertainty in the SA can again be taken as an upper limit on the extent of this emission region. For AS 205 N this is 2 au (after continuum subtraction), which equals 6 au when the inclination of the system is accounted for. Analysis of the [O I] λ6300 and [S II] λ6731 line regions reveals interesting results. As presented in Figure 3 the HVC3 and the HVC1 are displaced in the same direction while the HVC2 is displaced in the opposite direction. As HVC1 and HVC2 are both blueshifted one would expect them to be extended in the same direction if they are part of the same flow. The complex nature of the signals detected becomes clear in Figure 4, where the continuum subtracted results for perpendicular slits are combined to recover the PA of the signals. The four identified components are shown separately. The magenta line here marks the PA of AS 205 S with respect to AS 205 N. The red line gives the PA of the AS 205 N disk major axis. In [O I] λ6300 HVC2, HVC3, and HVC1, while offset in different directions, all lie along similar PA. The same directions are seen for the three HVCs in [S II] λ6731. Also note that the PAs of the extended components are very close to the binary PA and are also close to being perpendicular to the disk PA.

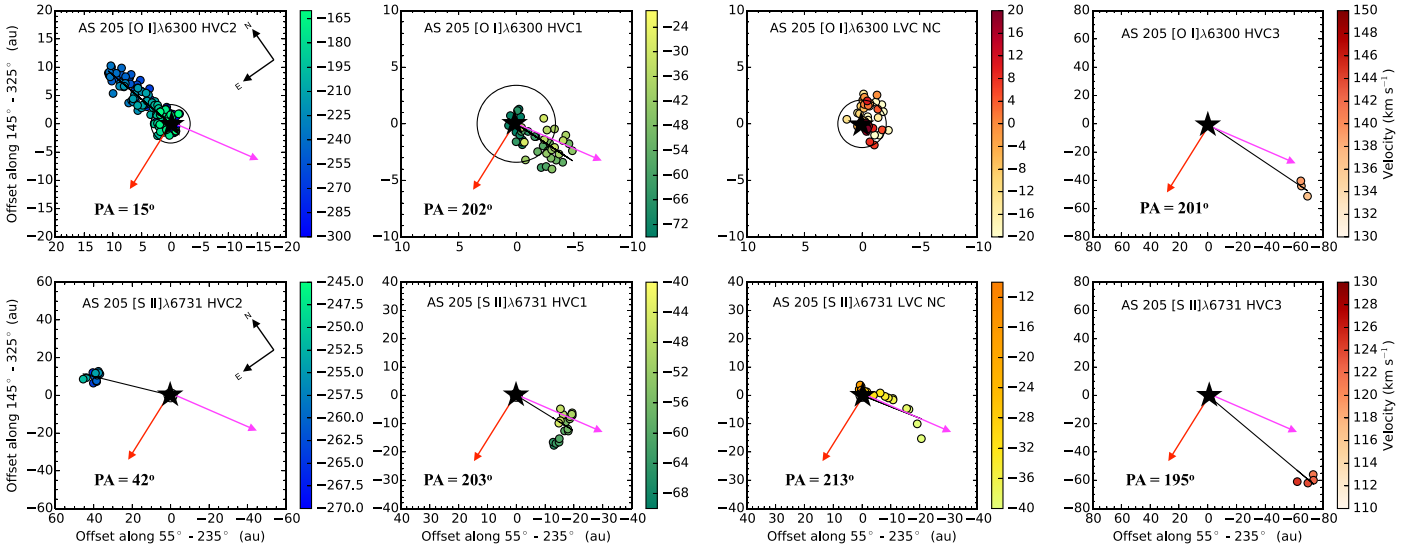

Figure 4. AS 205 N: Combining the perpendicular slit PAs to recover the 2D centroid at each wavelength (velocity). The continuum emission has been subtracted here to reveal the full offset in the outflow. The black circle is the 3σ uncertainty in the centroid, the red arrow the disk PA, the magenta arrow the binary PA, and the black arrow the best PA fit to the signals. These results are difficult to explain if the triple system is driving only one outflow.

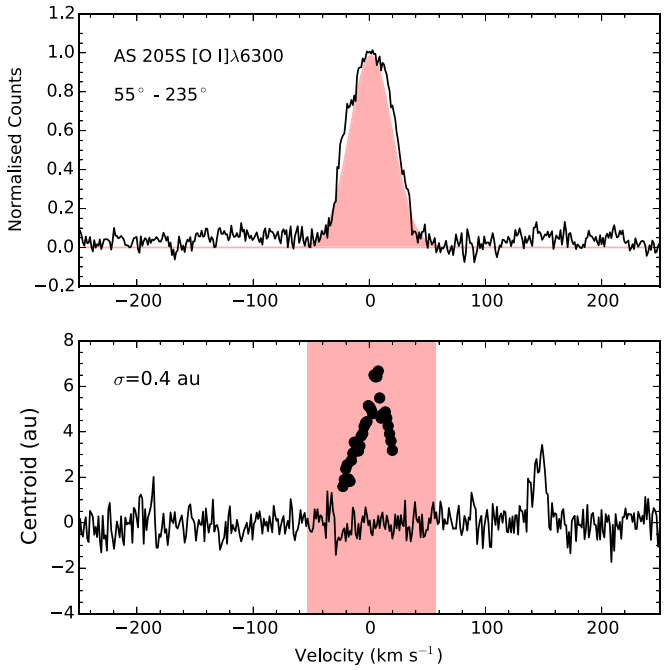

Figure 5. AS 205 S: spectroastrometric analysis of the [O I]λ6300 emission. Top: the continuum subtracted line emission, normalized to the line peak. The fitted kinematic component is overplotted. Bottom: the position spectrum with the range of the fitted LVC–BC shown as the colored shaded region. The continuum subtracted offsets are overplotted in black.

The analysis of the AS 205 S [O I] λ6300 line is presented in Figure 5. No [S II] λ6731 emission was detected for AS 205 S. No offset is measured for the [O I] λ6300 before continuum subtraction but there is a signal at the velocity of the redshifted emission detected for AS 205 N and in the direction of AS 205 N. After continuum subtraction this redshifted feature is located at $\sim$100 au from AS 205 S, in agreement with its location with respect to AS 205 N and the separation of $\sim$163 au between the two stars. Also the AS 205 S [O I] λ6300 emission line shifts in the direction of AS 205 N after continuum subtraction. In Figure 6, position–velocity diagrams of the [O I] λ6300 and [S II] λ6731 emission line regions are presented offering a further picture of the system. The location of the redshifted emission feature between the two sources is clear.

As noted, it is difficult to distinguish between a binary and outflow signal in this system. However, it is argued here that a likely explanation is that we are detecting an asymmetric jet ($V_{\rm blue} \sim -250\,{\rm km\,s^{-1}}$ and $V_{\rm red} \sim 140\,{\rm km\,s^{-1}}$) driven by AS 205 N, with the signals seen in HVC1, the [S II] λ6731 LVC and the AS 205 S [O I] λ6300 emission being binary signals. The redshifted jet emission is located beyond the shrouding effects of the disk. High angular resolution imaging in jet tracing lines could help to fully understand the outflow activity in the vicinity of the stars. We conclude that the nature of the LVC remains elusive until the flows can be disentangled and driving sources identified.

4. Discussion

As outlined above, spectroastrometry of visible spectra of RU Lupi and AS 205 N was previously presented by Takami et al. (2001, 2003). What is new about the analysis presented here is that the much improved spectral and spatial resolution (better seeing conditions) offered by observing with UVES, means that the different kinematical components that make up the forbidden emission can be easily distinguished and analyzed separately. Furthermore, the improved spectral resolution allows the relationship between displacement and velocity to be probed at a good resolution. In the case of AS 205 the improved seeing allows the N and S components to be separated. Another important development since the analysis by Takami et al. (2001, 2003) is the spectroastrometric analysis of the CO emission from both stars by Pontoppidan et al. (2011), who conclude that the CO fundamental at $\sim$4.7 μm is tracing a disk wind.

While the kinematic analysis of the RU Lupi and AS 205 N forbidden line emission summarized in Table 3 could suggest a similar spatial origin (within each component), the spectro-astrometric analysis presented in Figures 2 and 4 clearly points to a different origin. The important information to be taken

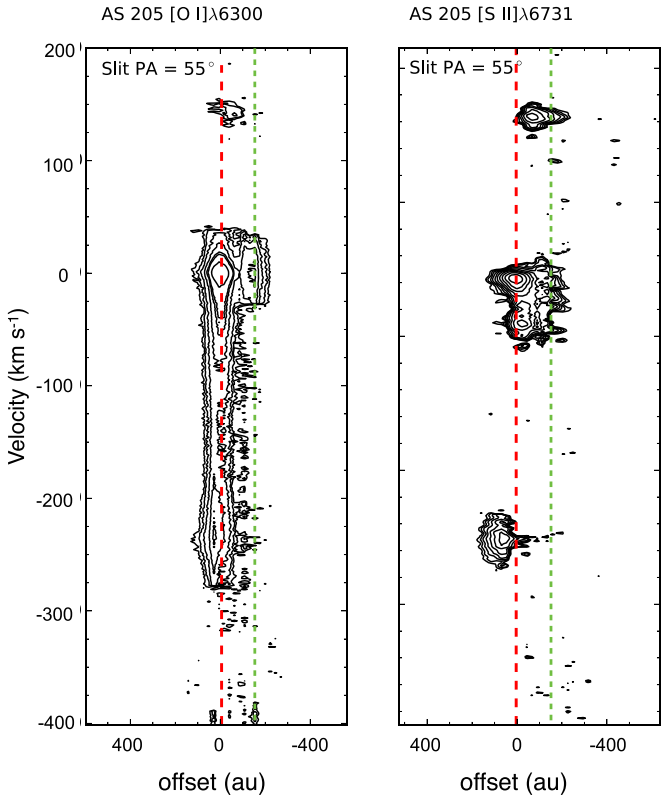

Figure 6. Continuum subtracted position–velocity diagram of the [O I] λ6300 and [S II] λ6731 emission from AS 205 for the 55° slit PA. Both AS 205 N and AS 205 S were included in the slit and the position of AS 205 S is marked with the green dashed line.

from these figures are the PAs of the extended emission and the relationship between velocity and displacement. From Figure 2, it is clear that the HVC2 (tracing the jet) and the LVC–NC have the same PA but for AS 205 N (Figure 4) the fastest component assumed to trace the jet (HVC2) and the displacement seen in the [S II] λ6731 LVC–NC are in opposite directions. The agreement in the PA of the different RU Lupi components is further highlighted in Figure 7. Here the different components are overplotted without the kinematical information given in Figures 2 and 4. The NCs are shown with filled blue symbols and the HVCs with unfilled green and red (AS 205 N) symbols. Green is chosen for the blueshifted HVCs to reflect the higher velocities with respect to the NCs. The agreement in PA for RU Lupi is striking while for AS 205 N the [S II] λ6731 NC and HVC1 are not straightforward to explain.

The distribution of the offsets with velocity also offer a clue to the origin of the emission. For the RU Lupi HVC2 there is a clear initial increase in velocity with displacement along the disk rotation axis, as would be expected for a collimated jet, while the LVC–NC velocity decreases with increasing vertical offset. This negative velocity gradient is seen in both [O I] λ6300 and [S II] λ6731 emission lines. Due to the complicated nature of the signals seen in AS 205 N the velocity distribution is less clear in Figure 4, although the HVC2 in [O I] λ6300 and the LVC–NC in [S II] λ6731 do show a positive gradient (an increase in offset with velocity), while the HVC1 shows a negative gradient in the [O I] λ6300. To further clarify how the velocities are distributed with distance for the LVC–NCs, the spatial offsets along the outflow PAs, as a function of velocity, are plotted in Figure 8. In Figures 2 and 4 the offsets shown were not deprojected but they are in Figure 8. The plotted offset is therefore the height above the circumstellar disk (z).

Observations of TT jet's forbidden emission line regions have clearly shown that there is an initial increase in the velocity of the jet with a distance from the driving source and this behavior was first recorded by Hirth et al. (1997). Decreases in velocity at individual knots in the jets are also observed highlighting the complicated knotty structure of the jets. Takami et al. (2001) note a similar behavior in the Hα and FEL regions of RU Lupi. They point out that this would be an expected feature of magnetically driven flows and use this as supporting evidence for the origin of the extended Hα emission in the RU Lupi outflow. This jet-like behavior is found here for the HVC2 component in RU Lupi, and we conclude that this is also found for all the AS 205 N components except for the HVC1 component in [O I] λ6300.

The RU Lupi LVC–NC is clearly showing something very different to what would be expected for a jet. Not only does it show a negative gradient in z but the gradient is much smoother and does not show evidence of regions of acceleration and deceleration as might be expected for shocked emission. In agreement with previous work, we find that a likely explanation of the velocity gradient is emission in an uncollimated MHD disk wind. The gradient seen in the RU Lupi NC was hinted at in the Takami et al. (2001) results. Takami et al. (2001) also investigated the velocity field of the RU Lupi [O I] λ6300 and [S II] λ6731 low-velocity emission and Figure 8 here can be directly compared to their Figure 3. Based on their data in Figure 3 of their article, Takami et al. (2001) conclude that the [O I] λ6300 LVC does not show a gradient and argue that this is consistent with the origin in a moderately collimated MHD disk wind. For the [S II] λ6731 line they note a slight positive gradient, which they say is due to blending between the HVC and LVC. Therefore, they cannot draw any conclusions about the [S II] λ6731 LVC gradient. The spectra analyzed in Takami et al. (2001) were taken with the RGO spectrograph on the AAT telescope at a much poorer spectral resolution than what was achieved here and so while they see a hint of what we find here in the [O I] λ6300 line it is likely that the [S II] λ6731 LVC was not resolved from the HVC.

The extent of the emission regions can also be deduced from Figure 8. While the displacements shown in Figures 1–5 were corrected for the continuum contamination they did not take the inclination of the systems into account. In Figure 8 the displacements along the measured jet PA are plotted and they are also deprojected. For RU Lupi both the LVC–NC and HVC2 are displaced further in [S II] λ6731 than in [O I] λ6300, as expected. From Figure 8 the RU Lupi NC is displaced as far out as $\sim$8 au and $\sim$40 au in [O I] λ6300 and [S II] λ6731, respectively, giving one of the first true measurements of the spatial extent of the LVC. The error on the measurement is given by the precision of the technique. The 1σ uncertainty is 0.6 au for [O I] λ6300 and 1 au for [S II] λ6731.

Figure 9 compares the results from this work with the spectroastrometric analysis of the CO emission from both stars presented by Pontoppidan et al. (2011). For both sources the HVC1 and LVC–NC components are delineated by vertical lines with the [S II] λ6731 components represented by a dashed line. The same color scheme as shown in previous figures is followed. We find that the RU Lupi CO results agree with the FELs while there is no such agreement for AS 205 N. The

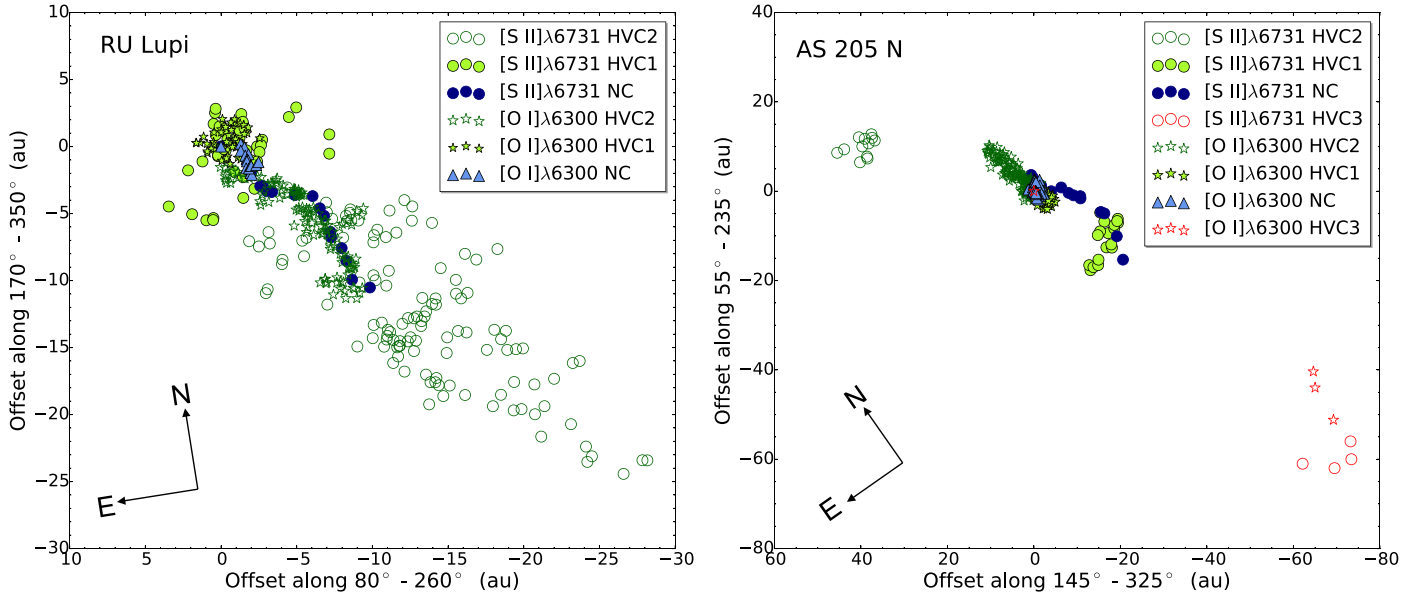

Figure 7. Comparing the spatial properties of the different kinematical components. For the blueshifted components the HVCs are shown in green to represent their larger velocity. The black stars show the stellar positions. The agreement in the PA of the different RU Lupi components is clear while in the case of AS 205 N the [S II] λ6731 NC and HVC1 do not agree with the idea of there being one outflow, as they are clearly in the direction of the redshifted flow.

comparison between the CO and FEL results for AS 205 N do show the signatures to be similarly shaped but then are along opposite PAs. Pontoppidan et al. (2011) model their CO spectroastrometric results as being produced by a wide-angled wind and they also see the negative gradient detected here.

Since the RU Lup disk is at a low inclination angle, the line-of-sight velocity measures largely the velocity component along the disk rotation axis (z direction). A negative gradient in this velocity with z therefore implies a decreasing v_z and for a wind this is consistent with a decreasing flow velocity with distance from the star and/or with a decrease in the collimation angle of the flow streamline, which also results in a decrease in the v_z component of the flow velocity. Both of these are predicted by MHD disk wind models. A similar fall off in velocity with disk radius has been observed in TT jets, where an "onion-like" velocity structure with fast-flowing gas enclosed by slower less collimated gas has been observed (see Frank et al. 2014 and references within). This interpretation of the negative velocity gradient is also consistent with the conclusion of Fang et al. (2018) that while the BCs trace disk radii within 0.5 au and heights (∼0.15 au) close to the disk (not detected in the UVES data), the NCs trace gas originates in a more extended wind at several au. Figure 10 is a sketch of how properties of the outflows from RU Lupi result in the spectro-astrometric offsets presented in Figures 1 and 2.

Our findings are very relevant to the ongoing debate about the origin of the LVC emission. Simon et al. (2016) found that the combination of blueshifts in the centroid and large FWHM of the LVC–BC pointed to an MHD disk wind origin while the origin of the NC was much less clear and a photoevaporative wind could not be ruled out, see also Ercolano & Owen (2016). As Banzatti et al. (2019) found that both the BC and NC kinematics were correlated, they further argued that they both are part of the same MHD wind and they put a constraint of 35° on the wind opening angle. While Weber et al. (2020) claimed that these same correlations can be achieved in an MHD inner wind (producing the HVC and BC) plus an X-ray driven photoevaporative wind (giving rise to the NC), the predicted [S II] λ6731 line luminosities are orders of magnitude larger than observed, see discussion in Pascucci et al. (2020), casting doubts on their proposed scenario.

We note that while a declining flow velocity with disk radius and poor collimation is also expected with photoevaporation, a photoevaporative flow for the origin of the RU Lupi NC is very unlikely. First, the observed blueshifts of $\sim$30 km s^{-1} at low z are too high to be consistent with photoevaporative flows, which, instead, predict shifts at thermal speeds of 5–10 km s^{-1} (Ballabio et al. 2020). Second, the [O I]λ6300 emission can be traced down to a vertical height z of $\lesssim$2 au from the disk midplane,[10] see Figure 8, with the wind being launched relatively deep within the gravitational potential well of the star.

We conclude, from the analysis of the velocity distribution of the different components and the comparison with the CO that the RU Lupi NC is most likely tracing an MHD disk wind. Gangi et al. (2020) compare molecular Hydrogen emission at 2.12 μm with the [O I] λ6300 emission from a sample of TTSs and conclude that the H_2 and [O I] λ6300 LV NC traces the same wind but cannot distinguish between a photoevaporative and an MHD wind. We also note the recent ALMA observations detected a nonKeplerian envelope in ^{12}CO, extended from the RU Lupi disk, which Huang et al. (2020) comment could be the colder/radially-extended counterpart of the inner MHD wind inferred in the CO fundamental line. The forbidden emission investigated here probes material closer to the fundamental CO emission, raising the interesting possibility of disk winds being present at nearly all disk radii. While it appears that the CO is tracing part of the blueshifted outflow of AS 205 N the situation is uncertain for the FEL HVC1 and LVC–NC. Salyk et al. (2014) also introduced some uncertainty as to whether the

[10] The [O I] λ6300 NC emission extends back closer to the star than the [S II] λ6731 emission but this is due to the lower critical density of the [S II] λ6731 line.

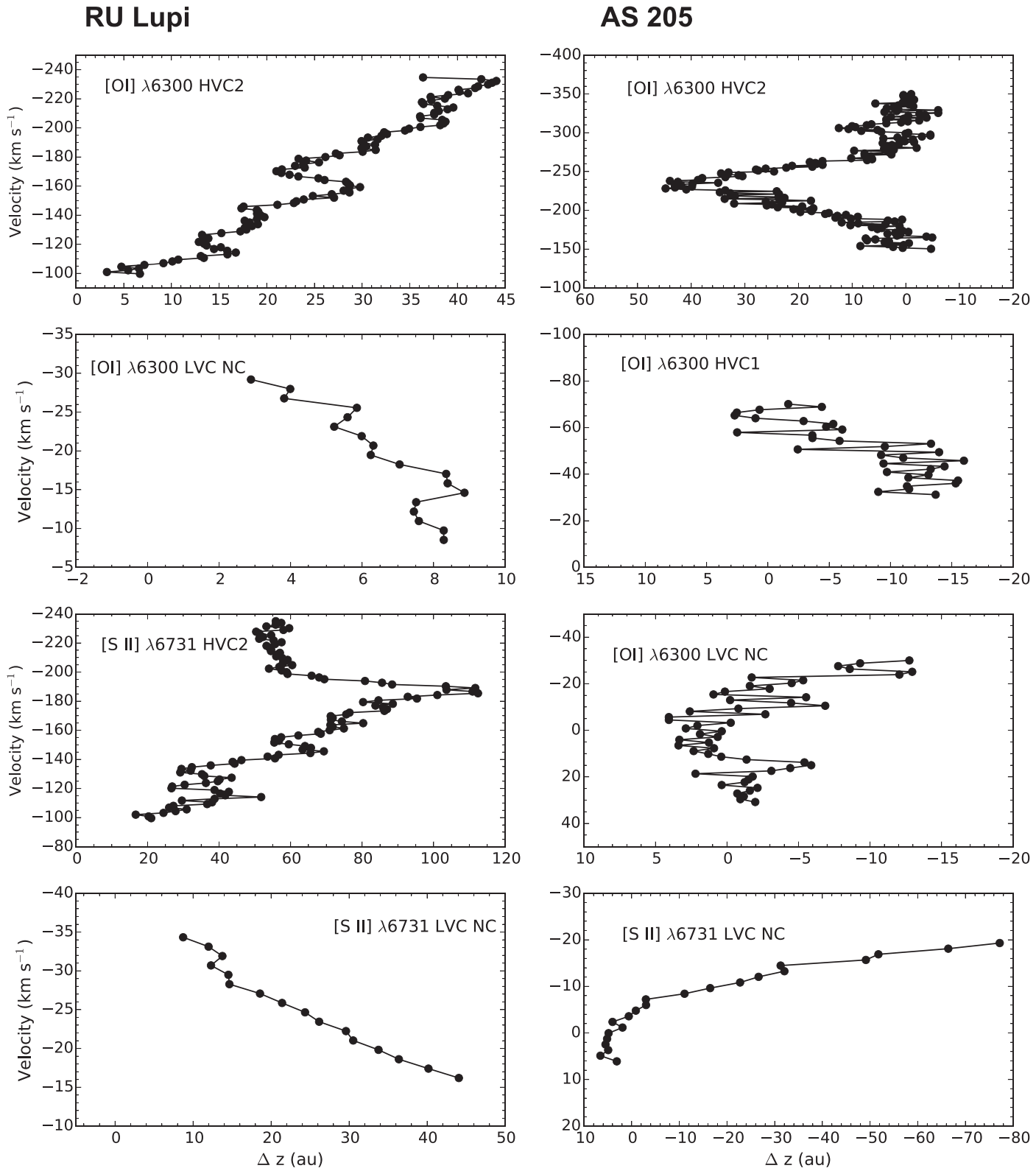

Figure 8. Deprojected spatial offset along outflow PA as a function of radial velocity for the RU Lupi and AS 205 N HVCs and HVCs and LVC–NCs. These results were extracted from Figures 2 and 4, and are the average of the results for the two sets of perpendicular slit PAs. RU Lupi: while the jet shows a general trend of an initial increase in velocity with distance (typical of TT jets) a negative gradient is seen in the LVC–NC emission. AS 205 N: for all components except the [O I] λ6300 HVC1 an initial increase in displacement with velocity is seen. This could be due to mixing between the HVC1 and HVC2, which are displaced in opposite directions.

CO is tracing a disk wind in AS 205 N as they suggest that the CO spectroastrometric signature could have been confused by the binary. Further investigation is needed to disentangle the complicated outflow emission from the AS 205 system. As a wide-angled wind would enclose the fast collimated jet (Klaassen et al. 2013), it would be expected that the PA of the wind component would be found to be the same as the PA of the jet in AS 205, as seen for RU Lupi.

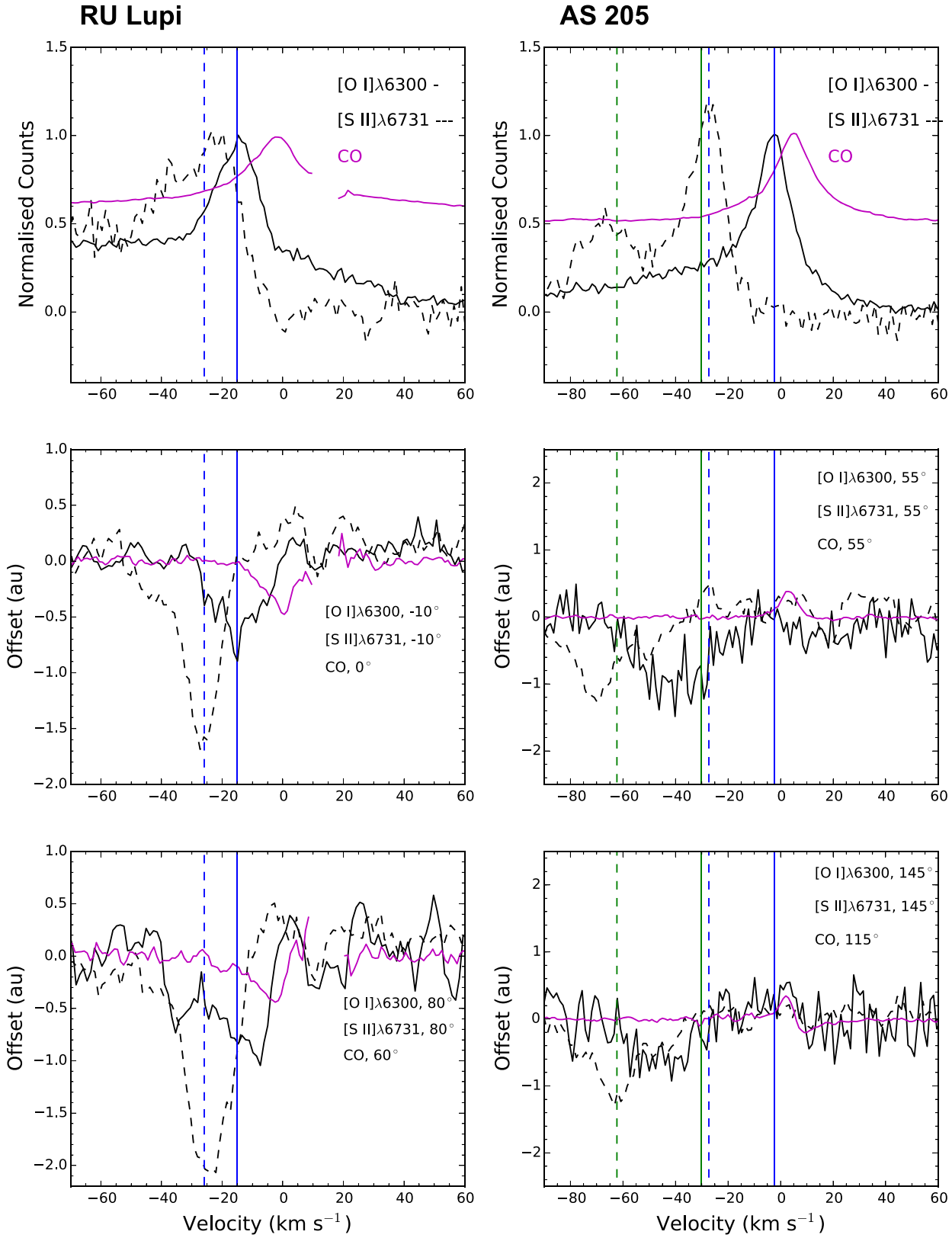

Figure 9. Comparison of the RU Lupi and AS 205 N spectroastrometric results for the LVC–NC to what was found for the CO by Pontoppidan et al. (2011). The CRIRES CO spectra and the UVES spectra were taken at different slit PAs, so the spectra closest in PA are compared. Also the CO results were not corrected for continuum subtraction and so what is compared is the offsets measured before continuum subtraction and what is shown in Figures 1 and 3. The vertical lines mark the velocities of the forbidden line NCs and HVC1s in both sources. They are shown dashed for the [S II]λ6731 line. RU Lupi: the shape of the offsets is similar between the two lines. The maximum offset is at the peak of the line and then offset gradually tails off as velocity increases. This shows that the LVC–NC of the FELs and CO have the same origin. AS 205 N: unlike what is found for RU Lupi there is no agreement between the FEL and CO results here emphasizing that an MHD disk wind is not detected in this case.

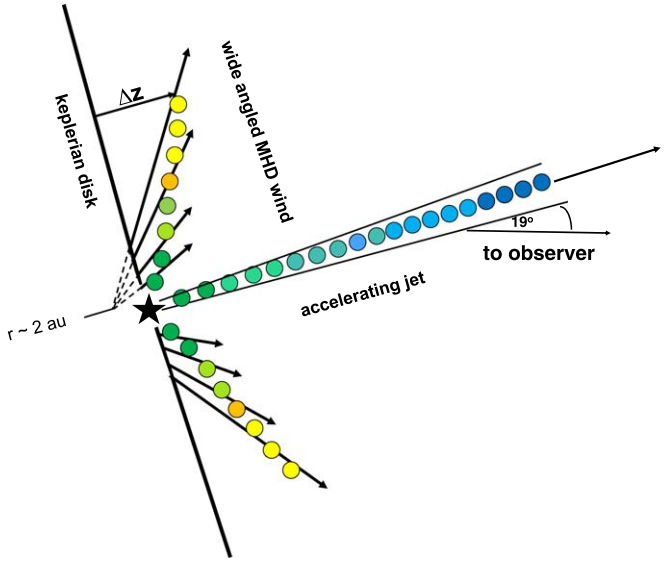

Figure 10. Sketch illustrating how the spectroastrometric signals presented in Figures 1 and 2 are tracing the outflows from RU Lupi. The colored dots are the positional displacements shown in Figure 2 with the colors from yellow (0 km s^{-1}) to dark blue (−230 km s^{-1}) representing increasing velocities. The HVC2 is tracing the accelerating jet with velocities from −90 to −230 km s^{-1}. The LVC–NC is tracing a wide-angled MHD disk wind with a velocity range of −40–0 km s^{-1}. For the MHD wind component, the velocity of each point corresponds to flow streamline and therefore a disk radius r. The spectroastrometric technique is recording the height of the emission above the disk z at each velocity (or r). As the velocity is decreasing with increasing r and z is increasing with r, the spectroastrometric results shown in Figure 2 for the NC have a negative velocity gradient.

5. Summary and Conclusions

We carried out UVES spectroastrometry in the different kinematic components of the [O I] λ6300 and [S II]$\lambda\lambda$ 6716, 6731 from two accreting stars, RU Lupi, and AS 205 N. For AS 205 N several outflow components were revealed indicating the presence of at least two outflows, which is not surprising given that it is a multiple system. Analysis of the relationship between velocity and offset for the different AS 205 N flow components generally showed them to be jet-like. For RU Lupi a clear jet component was detected (HVC2, $V \sim -195$ km s^{-1}), which showed an increase in velocity with distance and evidence of a knotty structure. Another HVC component (HVC1, $V \sim -66$ km s^{-1}) shows no offset and we argue that it traces the base of the jet. The most significant finding was for the RU Lupi LVC–NC that was found to be extended along the same PA as the jet (to a distance of ∼40 au in [S II] λ6731) but with a negative velocity gradient. This is opposite to the behavior seen for jets. The evidence extracted from the spectroastrometric analysis for RU Lupi and the comparison with a previous spectroastrometric study of CO emission points to an origin in a disk wind for the RU Lupi NC. This is the first clear evidence of spatially resolved emission in an MHD disk wind for an LVC–NC in an FEL and one of the first measurements of the wind height. Furthermore, this work highlights that a kinematical study alone is not enough to clarify the origin of the different velocity components. From the kinematical analysis alone, the FEL regions of both stars seems similar, but spectroastrometry tells a different story. This approach should now be extended to a greater sample of objects to see if the LVC–NC routinely traces a disk wind or if indeed RU Lupi is a unique object.

This work is based on data collected by UVES (089.C-0299) observations at the VLT on Cerro Paranal (Chile), which is operated by the European Southern Observatory (ESO). We thank Klaus Pontoppidan for providing the CO position spectra originally published in Pontoppidan et al. (2011). Emma Whelan would like to acknowledge support from The Maynooth University Seed Fund 2019. I.P., U.G., and S.E. acknowledges support from a Collaborative NSF Astronomy & Astrophysics Research grant (ID: 1715022, ID:1713780, and ID:1714229). R.D.A. acknowledges funding from the European Research Council (ERC) under the European Union's Horizon 2020 research and innovation program (grant agreement No. 681601).

Appendix
[O I] λ6300 Variability

The [O I] λ6300 emission in RU Lupi and AS 205 N were previously investigated in Banzatti et al. (2019) and Fang et al. (2018). Both studies examined the same data sets, which are the Keck/HIRES archival spectra taken in 2008. In Table 4 the results of the kinematical fitting in these works are compared to our results. Both works identify an LVC broad and narrow component and two blueshifted HVCs for both sources, although for RU Lup the centroid and FWHM for the BC and one HVC are significantly different (see Table 4)[11]. Banzatti et al. (2019) outline the changes in their approach to the kinematical fitting, which accounts for these differences. The main difference between the results of this paper and these previous works is that no LVC–BCs are identified. In Figure 11 we compare the normalized HIRES and UVES [O I] λ6300 line profiles with the UVES. Note that at the epoch of the UVES observations the high-velocity emission has changed in both sources. This, in combination with the complex [O I] λ6300 profiles, leads us to identify different Gaussian components than those published. Most notably, following the 30 km s^{-1} separation for the LVC and HVC (e.g., Simon et al. 2016), we do not identify the weaker and more blended LVC–BC in the UVES spectra.

[11] Note that Banzatti et al. (2019) report in their tables only the most blueshifted HVC but complete fits are available here: http://distantearths.com/Ilaria/disk-winds/.

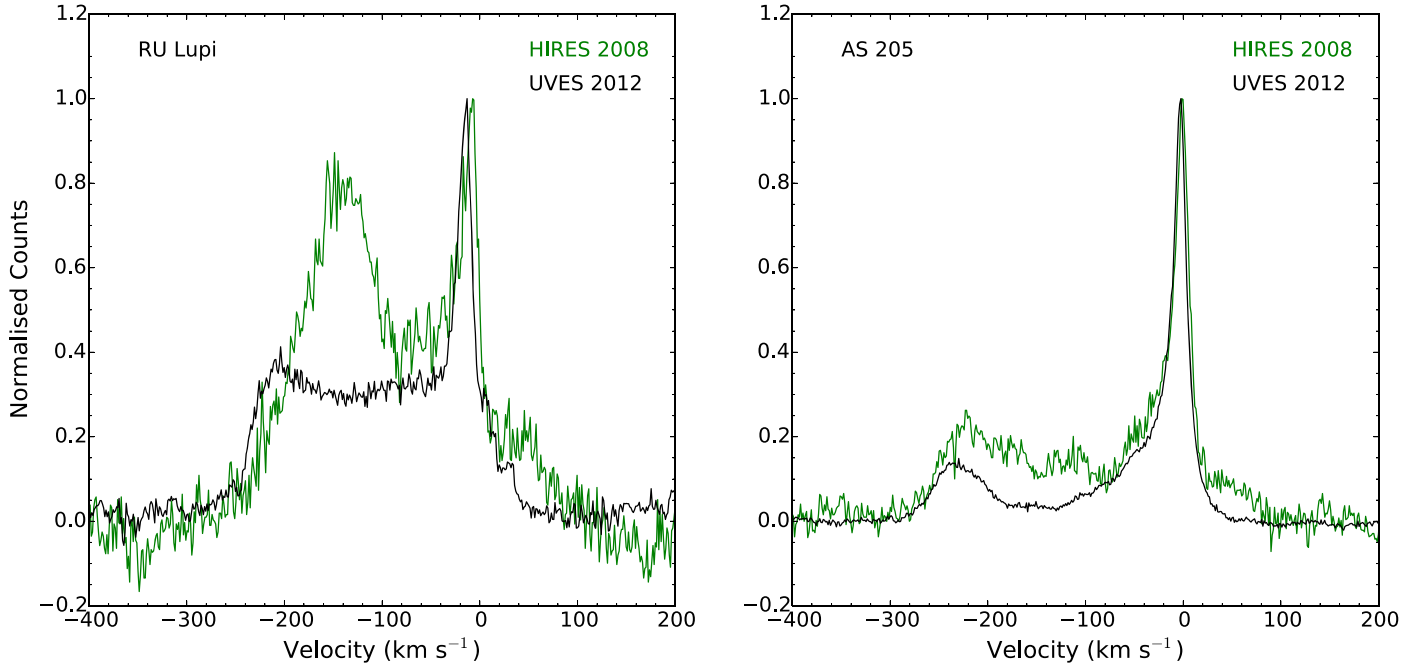

Figure 11. A comparison of the [O I] λ6300 line profile in the HIRES (green) and UVES (black) spectra. In both cases the high-velocity emission has decreased and this is most striking for RU Lupi.

Table 4
Comparison of the [O I] λ6300 Decomposition from Fang et al. (2018) and Banzatti et al. (2019) to Our Own Kinematic Decomposition (Last Column)

	Fang 2018 $V_{\rm rad}$, FWHM (km s^{-1})	Banzatti 2019 $V_{\rm rad}$, FWHM (km s^{-1})	UVES $V_{\rm rad}$, FWHM (km s^{-1})
RU Lup			
	LVC–NC (−10.9, 13.9)	LVC–NC (−12, 15)	LVC–NC (−13.0, 18.2)
	LVC–BC (−10.1, 176.4)	LVC–BC (−36, 44)	not identified
	HVC (−32.3, 40.5)	HVC (−60, 292)	HVC (−66.0, 150.0)
	HVC (−149.4, 109.9)	HVC (−148, 80)	HVC (−197.5, 59.5)
AS 205 N			
	LVC–NC (−0.7, 14.5)	LVC–NC (−0.4, 14.5)	LVC–NC(−2.3, 16.8)
	LVC–BC (−13.5, 54.5)	LVC–BC (−14.4, 54)	not identified
	HVC(−85.4, 225.5)	not identified	HVC (−30.3, 88.2)
	HVC (−221.9, 56.3)	HVC (−223, 58)	HVC (−226.5, 76.4)
	not identified	not identified	HVC (139.5, 13.7)

ORCID iDs

E. T. Whelan https://orcid.org/0000-0002-3741-9353
I. Pascucci https://orcid.org/0000-0001-7962-1683
U. Gorti https://orcid.org/0000-0002-3311-5918
S. Edwards https://orcid.org/0000-0002-3232-665X
R. D. Alexander https://orcid.org/0000-0001-6410-2899
M. F. Sterzik https://orcid.org/0000-0002-5784-4437

References

Armitage, P. J. 2011, ARA&A, 49, 195
Bai, X.-N., & Stone, J. M. 2013, ApJ, 769, 76
Bailey, J. 1998, MNRAS, 301, 161
Balbus, S. A., & Hawley, J. F. 1991, ApJ, 376, 214
Ballabio, G., Alexander, R. D., & Clarke, C. J. 2020, MNRAS, 496, 2932
Banzatti, A., Pascucci, I., Edwards, S., et al. 2019, ApJ, 870, 76
Brannigan, E., Takami, M., Chrysostomou, A., & Bailey, J. 2006, MNRAS, 367, 315
Cahill, E., Whelan, E. T., Huélamo, N., et al. 2019, MNRAS, 484, 4315
Curran, R. L., Argiroffi, C., & Sacco, G. G. 2011, A&A, 526, A104
Dekker, H., D'Odorico, S., Kaufer, A., Delabre, B., & Kotzlowski, H. 2000, Proc. SPIE, 4008, 534
Edwards, S., Cabrit, S., Strom, S. E., et al. 1987, ApJ, 321, 473
Ercolano, B., & Owen, J. E. 2016, MNRAS, 460, 3472
Ercolano, B., & Pascucci, I. 2017, RSOS, 4, 170114
Fang, M., Pascucci, I., Edwards, S., et al. 2018, ApJ, 868, 28
Frank, A., Ray, T. P., Cabrit, S., et al. 2014, Protostars and Planets VI (Tucson, AZ: Univ. Arizona Press), 451
Gaia Collaboration, Brown, A. G. A., Vallenari, A., et al. 2018, A&A, 616, A1
Gangi, M., Nisini, B., Antoniucci, S., et al. 2020, A&A, 643, A32
Gressel, O., & Pessah, M. E. 2015, ApJ, 810, 59
Hartigan, P., Edwards, S., & Ghandour, L. 1995, ApJ, 452, 736
Hartigan, P., & Morse, J. 2007, ApJ, 660, 426
Hirth, G. A., Mundt, R., & Solf, J. 1997, A&AS, 126, 437
Huang, J., Andrews, S. M., Dullemond, C. P., et al. 2018, ApJL, 869, L42
Huang, J., Andrews, S. M., Öberg, K. I., et al. 2020, ApJ, 898, 140
Klaassen, P. D., Juhasz, A., Mathews, G. S., et al. 2013, A&A, 555, A73
Koenigl, A., & Ruden, S. P. 1993, Protostars and Planets III (Tucson, AZ: Univ. Arizona Press), 641
Kurtovic, N. T., Pérez, L. M., Benisty, M., et al. 2018, ApJL, 869, L44
McCabe, C., Ghez, A. M., Prato, L., et al. 2006, ApJ, 636, 932

McGinnis, P., Dougados, C., Alencar, S. H. P., et al. 2018, A&A, 620A, 87
Nisini, B., Antoniucci, S., Alcalá, J. M., et al. 2018, A&A, 609, A87
Pascucci, I., Banzatti, A., Uma, G., et al. 2020, ApJ, 903, 78
Pontoppidan, K. M., Blake, G. A., & Smette, A. 2011, ApJ, 733, 84
Rigliaco, E., Pascucci, I., Gorti, U., et al. 2013, ApJ, 772, 60
Salyk, C., Pontoppidan, K., Corder, S., et al. 2014, ApJ, 792, 68
Salyk, C., Pontoppidan, K. M., Blake, G. A., et al. 2008, ApJL, 676, L49
Simon, M. N., Pascucci, I., Edwards, S., et al. 2016, ApJ, 831, 169
Takami, M., Bailey, J., & Chrysostomou, A. 2003, A&A, 397, 675
Takami, M., Bailey, J., Gledhill, T. M., et al. 2001, MNRAS, 323, 177
Weber, M. L., Ercolano, B., Picogna, G., Hartmann, L., & Rodenkirch, P. J. 2020, MNRAS, 496, 223
Whelan, E., & Garcia, P. 2008, Jets from Young Stars II (Berlin: Springer-Verlag), 123
Whelan, E. T., Huélamo, N., Alcalá, J. M., et al. 2015, A&A, 579, A48